RSC Advances

PAPER

Cite this: *RSC Adv.*, 2018, **8**, 15813

Synthesis and application of hydrophilically-modified Fe_3O_4 nanoparticles in oil sands separation†

Zisheng Zhang,‡[abc] Hongda Li,‡[ab] Hong Sui,[abd] Lin He *[ab] and Xingang Li[abd]

Nanoparticles have been reported to be a promising candidate for the separation of heavy oil from its host rock's surface. These nanoparticles (NPs) are often dispersed and stabilized in the solution by some surfactants during the unconventional oil ores processing. Herein, the PEG600–KH560 (PK) has been grafted onto Fe_3O_4 NP surfaces, obtaining a kind of hydrophilically-modified recyclable nanoparticle. Results show that these NPs (averaged at around 16 nm for single sphere) could be well dispersed in water (no settling in 72 h), forming PK-Fe_3O_4 nanofluids (NFs) at 0.2 wt%. These PK-Fe_3O_4 NFs are found to be able to be quickly separated from the dispersions by an external magnetic field, and returning back to stable NFs when the magnetic field disappears and by shaking. The PK-Fe_3O_4 NFs have been further used for the enhancement of heavy oil recovery from oil sands. The floatation results show that the PK-Fe_3O_4 NFs could improve oil recovery by at least 12% compared with the traditional hot water extraction process (HWEP). After the extraction, up to 70% of the PK-Fe_3O_4 NPs could be directly recycled from the solution for further use. The rest of the NPs are left in the oil phase and attached on the residual solid surface. However, the efficiency of the PK-Fe_3O_4 NPs is found to be decreased when the recycling times exceed 5 due to the adsorption of oil components. A mechanistic study shows that the hydrophilic PK-Fe_3O_4 NPs could be adsorbed on the mineral surface, making the surface more hydrophilic. The hydrophilic surface and the agitation disturbance helps the liberation process of bitumen from the solid surfaces. On the other hand, when adding the PK-Fe_3O_4 NPs into the heavy oil–water system, the oil–water interface is found to be highly modified by the NPs, resulting in significant reduction of the oil–water interfacial tension. The above findings suggest that the PK-Fe_3O_4 NPs combined the surface-active role (surfactant) and the nano-size role (adsorption) together, which facilitates its role in oil sands separation.

Received 6th March 2018
Accepted 19th April 2018

DOI: 10.1039/c8ra01966e

rsc.li/rsc-advances

1. Introduction

With proven reserves of more than 6 trillion of barrels, the unconventional oil accounts for a major part of fossil fuel resources. Many technologies, including steam extraction, pyrolysis, chemical flooding, solvent or vapor extraction, emulsion flooding, and microorganism application have been proposed to recover the heavy oil from unconventional oils.[1–4] The chemical flooding is the most used method for tertiary oil recovery or enhanced oil recovery (EOR). The chemicals involved during the flooding process are mainly chemical surfactants, bio-surfactants, salts, nanoparticles, polymers, or even gases.[5–9] These chemicals are used to reduce the oil–water interfacial tension, to decrease oil viscosity or expand oil volume, to increase the effectiveness of water flooding.[10] The application of nano materials has shown potential to solve different problems in oil and gas industry.[11,12] Nanoparticles (NPs) have been utilized in subsurface applications due to their ability to alter certain properties in the unconventional oil ores. NPs exhibit exceptional properties compared with other chemicals owing to the small size and large surface area.[1,13]

During the past years, different kinds of NPs have been applied in enhanced oil recovery, such as SiO_2, Al_2O_3, TiO_2, ZrO_2, Fe_2O_3, nanoclay, *etc.*[7,14–16] These NPs are often dispersed in the water solution together with some surfactants to form nanofluids (NFs), which are further used to extract the oil from the oil matrix.[14,15,17,18] It is reported that the efficiency of NPs in heavy oil recovery is highly dependent on the NPs types, NPs concentration, temperature, pH, surfactants, and salinity of

[a]*School of Chemical Engineering and Technology, Tianjin University, Tianjin 300072, China. E-mail: linhe@tju.edu.cn*

[b]*National Engineering Research Centre for Distillation Technology, Tianjin 300072, China*

[c]*Department of Chemical and Biomedical Engineering, University of Ottawa, Ottawa, ON K1N 6N5, Canada*

[d]*Collaborative Innovation Center of Chemical Science and Engineering (Tianjin), 300072, China*

† Electronic supplementary information (ESI) available. See DOI: 10.1039/c8ra01966e

‡ These authors contribute equally to this work.

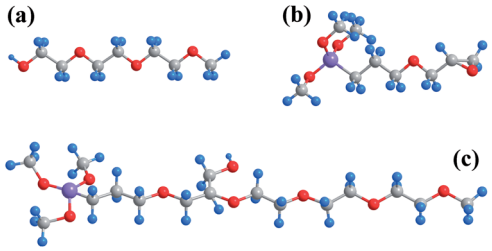

Fig. 1 Stick model of (a) PEG600; (b) KH560; (c) PEG600–KH560 molecule (sketch map), blue, grey, red and purple balls stand for hydrogen, carbon, oxygen and silicon atoms, respectively.

water.[10,13–16,18–20] For example, about an extra of 26 wt% of oil recovery is obtained when silica NPs are added into the solution at 3 wt%.[17] Mohebbifar *et al.*[6] applied 3000 ppm silica NFs with xanthan (a biopolymer) as thickening agent. They found that about 78 wt% of the coated Iranian heavy oil could be replaced by the NFs from the glass surface. The main roles of NPs for enhanced oil recovery are proposed to be the wettability alteration,[10,14,15,17,20–22] interfacial tension (IFT) reduction,[13,22–24] viscosity influence,[7,23–25] high disjoining pressure by vessel structure and spontaneous imbibition.[10,13,26–29] However, the exact mechanisms of the NPs in extracting oil, especially the unconventional oils, are still unclear.

Although much progress has been achieved, there are still many challenges before the commercialization of NPs in oil production. One of the main problems is the high cost of the NPs. There would be several ways to reduce the operational cost of NPs enhanced oil recovery: using cheaper NPs, reducing the dosage, recycling the NPs. Among these methods, the recycling of NPs is a promising method for the reduction of the operational cost. The Fe_3O_4 nanoparticle is a kind of ferrous nanoparticle. Except for general advantages in small size and high surface energy, Fe_3O_4 nanoparticle has a superparamagnetic feature, allowing it to be recyclable by magnetic separation. This recyclability of Fe_3O_4 NPs makes the possibility of reusing these NPs during the practical applications.

However, most of the reported NPs used in the oil recovery have a trend of self-aggregation due to their small size. To obtain a steady NFs system, different ways are proposed, such as surface modification,[26,30–34] combining surfactants,[35] bringing ultrasonication and pH adjustment. It is reported that the polymer-grafting is a promising choice for stabilizing NPs.[36] Sharma *et al.*[22] applied polyacrylamide (PAM) to graft onto SiO_2 NPs surface. The obtained NPs showed good stability in high-temperature environments. Sang *et al.*[37] used hydrophobically associative hygroscopic zwitterionic polymer to stabilize silica NPs. The fluidity of the complex oil could be improved with NFs flooding and 74.1% of oil could be recovered by modified NPs-based NFs in core flooding experiment.

Accordingly, in this work, we want to synthesize a multi-functional nanoparticle, possessing nano-size effect, chemical surface activity and recyclability. We plan to synthesize the Fe_3O_4 NPs which are grafted by a hydrophilic materials (*i.e.*, polyethylene glycol 600 (PEG600)). This grafting will make the surface of Fe_3O_4 NPs more hydrophilic, leading to its high dissolution and stabilization in water. Therefore, the purposes of this work are to: (i) synthesize PK-grafted Fe_3O_4 NPs and prepare PK-Fe_3O_4 NPs-based NFs; (ii) test the feasibility of PK-Fe_3O_4 NFs in separating bitumen from oil sands and (iii) understand the primary roles of PK-Fe_3O_4 NFs in oil–mineral separation.

2. Materials and methods

2.1. Materials

Chemicals, such as $FeCl_2 \cdot 4H_2O$ and $FeCl_3 \cdot 6H_2O$, were both purchased at analytical grade from Tianjin Jiangtian Chemical Technology Co., Ltd. 2,3-Epoxypropoxy propyltrimethoxysilicane (KH560) and polyethylene glycol 600 (PEG600), shown in Fig. 1a and b, were provided at analytical grade by Tianjin Heowns Biochemical Technology Co., Ltd. Ammonium hydroxide ($NH_3 \cdot H_2O$, 25%) was got from Tianjin Kemiou Chemical Reagent Co., Ltd. Canadian oil sands from Athabasca, Alberta was used in this study. The oil sands samples were

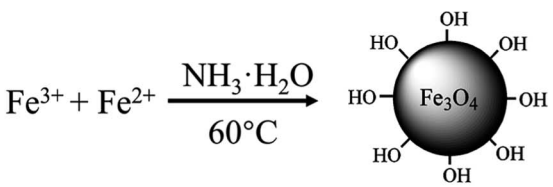

(1)

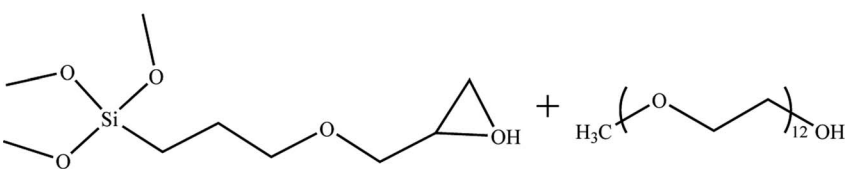

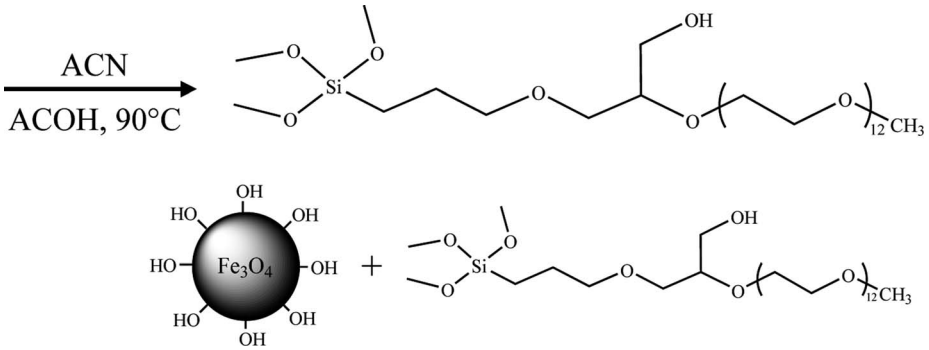

(2)

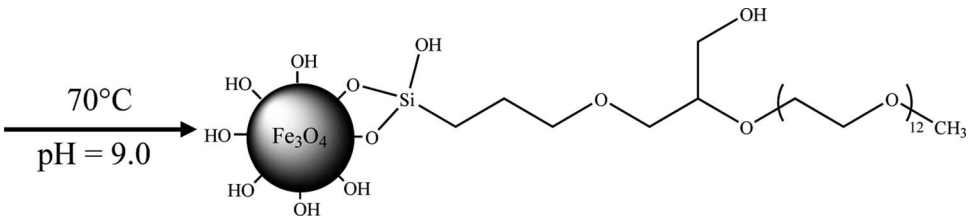

(3)

analyzed using the Dean–Stark standard method. The composition is determined to be as: 10.72 wt% bitumen, 1.79 wt% water and 87.49 wt% solids.

2.2. Synthesis of PK-Fe_3O_4 nanoparticles

The Fe_3O_4 NPs were synthesized by co-precipitation method on the basis of eqn (1).[38–40] $FeCl_2 \cdot 4H_2O$ and $FeCl_3 \cdot 6H_2O$ were dissolved in deionized water at molar ratio of 1 : 2. Ammonia (5 wt%) was added to adjust the pH of solution to 9.0. The whole reaction continued 30 min under nitrogen atmosphere at 60 °C. Then, a magnetic bar was used to separate the black Fe_3O_4 NPs from the solution, followed by washing with deionized water and alcohol twice. Finally, NPs were dried by vacuum freeze dryer for 24 h.

Then, the PEG600–KH560 (PK) was prepared by chemically linking PEG600 to KH560 on the basis of eqn (2). Firstly, to prevent the silane hydrolysis, PEG600 was dried at 80 °C for 3 h to remove water completely. Subsequently, 14.00 g of PEG600 was diluted by 150 mL of acetonitrile with the addition of 0.20 mL of acetic acid as catalyst. Then, 5.90 g of KH560 was added into the solution dropwise in 30 min. After refluxing at 90 °C with continuous stirring for 6 h, the products were separated from solvent by vacuum evaporation.

The PK molecules were grafted on Fe_3O_4 NPs, shown as eqn (3). The reaction details were given as follows: firstly, 1.50 g of PK was hydrolyzed by 75.0 mL of water at pH 9.50 for 30 min to produce silanol groups, and Fe_3O_4 NPs were dispersed in water at pH 9.50 by ultrasonication for 6 min. Secondly, the hydrolyzed agents were injected dropwise into 1.00 wt% Fe_3O_4 NFs suspension in 30 min. The mixture was then refluxed at 90 °C under nitrogen atmosphere and continuously stirred for 12 h. Finally, the products were collected from suspending medium by magnetic bar followed by twice washing with deionized water and alcohol and dried by heating at 80 °C for 6 h.

2.3. Preparation of PK-Fe_3O_4 nanofluids

The PK-Fe_3O_4 NFs were prepared by dispersing PK-Fe_3O_4 NPs into deionized water. Then, the prepared NFs (0.20 wt%) were stabilized with NaOH solution to adjust pH at 8.00. The NFs were further dispersed by ultrasonication for 30 min followed by being preserved in glass bottles. Visualization tests showed that no obvious settlement of NPs was observed in 72 h. Nanoparticle size analyzer and UV-vis test were further used to evaluate the stability of NFs in long-term experiments. The results of nanosizer test (shown in Fig. 2a) showed that the average size of NFs has an increase (from 47.3 nm to 95.0 nm) after free placing for 200 h at ambient temperature. The UV-vis test (shown in Fig. 2b) showed that the UV absorption of the NFs only had a little decrease (from 0.800 to 0.782 for original NFs and from 1.434 to 1.410 for recycled NFs) at the wavelength of 300 nm, suggesting the stability of NFs for further experiments.[41] Fig. 2a also indicated that the average size increased slightly after

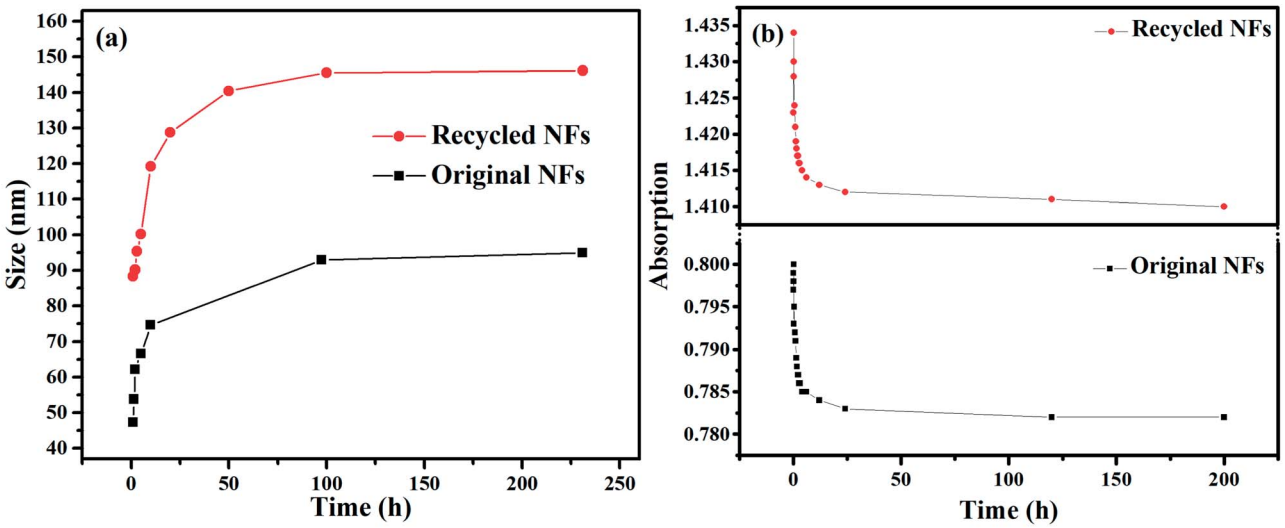

Fig. 2 (a) Size peaks of original and recycled NFs at different time intervals; (b) UV-vis absorption of original NFs and recycled NFs at 300 nm as a function of time.

placing for 48 h. Thus, the obtained NFs were freely placed for 48 h before using for enhancement of oil recovery, IFT tests and contact angle measurements.

2.4. Oil recovery by PK-Fe_3O_4 nanofluids

The PK-Fe_3O_4 NFs were used to separate the bitumen from oil sands by floatation in a Denver Floatation Cell. The procedures below were followed to collect bitumen froth samples:[42] firstly, the toluene (0.86 mL) was distributed evenly on oil sands sample (50.00 g) followed by a soaking time of 10 min to reduce the viscosity of oil sands bitumen.[43] PK-Fe_3O_4 NFs (1000 mL, 0.20 wt%) was prepared at pH 8.00. Secondly, the toluene-diluted oil sands ores were transferred into the floatation cell followed by the addition of NFs. The mixture was conditioned under 45 °C for 5 min at the stirring rate of 1500 rpm. After conditioning, air was injected at a flow rate of 150 mL min^{-1}. The floatation test was conducted for 15 min. A beaker was used to collect the froth samples, with samples collected at the end of 1 minute, 3 min, 5 min, 10 min and 15 min. Finally, the collected froth sample was transferred into a thimble, which would be further analyzed using Dean–Stark apparatus. On the basis of the extraction results, bitumen recovery and froth quality (B/S, bitumen to solids mass ratio) are calculated using the following equations:

$$R_b = \frac{m_f}{m_o} \times 100\% \quad (4)$$

$$Q_f = \frac{m_f}{m_s} \quad (5)$$

where, R_b, m_f, m_o, Q_f, and m_s present the bitumen recovery (%), the mass of bitumen in the froth (g), the mass of bitumen in the ore (g), B/S (mass ratio of the mass of bitumen in the froth and the mass of solid in the froth) and the mass of solid in the froth (g), respectively.

The NFs was recycled and reused by the following procedures: firstly, PK-Fe_3O_4 NPs were recycled from solution and tail sands by magnetic bar for 10 min. Secondly, the recycled NPs were washed by water and alcohol twice to separate the sands as much as possible. Finally, recycled NPs were dispersed into deionized water and the pH was adjusted to 8.00. The lost NPs were supplemented by parallel experiments to ensure the accuracy of the experiments.

2.5. Instrumental characterizations

The transmission electron microscopy (TEM, JEM 2010) and the scanning electron microscope (SEM, S4800) devices were used to investigate the morphology and homogeneity of Fe_3O_4 NPs and PK-Fe_3O_4 NPs. The open-loop reaction between KH560 and PEG600 and the grafting reaction between PK molecule and Fe_3O_4 NPs were monitored by the Fourier transform infrared spectroscopy (FT-IR, Tensor II) using the Attenuated Total Reflection (ATR) method. Powder X-ray diffraction (XRD) and X-ray photoelectron spectra (XPS) patterns of Fe_3O_4 NPs and PK-Fe_3O_4 NPs were collected on D8 advance diffractometer and 250xi photoelectron spectrometer, respectively. The magnetic properties of the two NPs were measured on a Lake Shore 7404 vibrating sample magnetometer (VSM) at ambient temperature. The thermogravimetric Analysis (TG, TGA/DSC1) was applied to record thermal stability and surface grafting characterization of the two NPs with a heating rate of 10 °C min^{-1} from 40 to 800 °C under nitrogen atmosphere. The size distribution and zeta potentials of PK-Fe_3O_4 NFs were evaluated by nanoparticle size analyzer (Nano ZS, Malvern). The ultraviolet and visible spectrophotometer (UV-vis, TU-1810) was used to evaluate the stability of NFs and to check samples obtained from floatation experiment. X-ray fluorescence spectroscopy (XRF, S4 Pioneer) was used to test element contents of sands after extraction process in Dean–Stark apparatus.

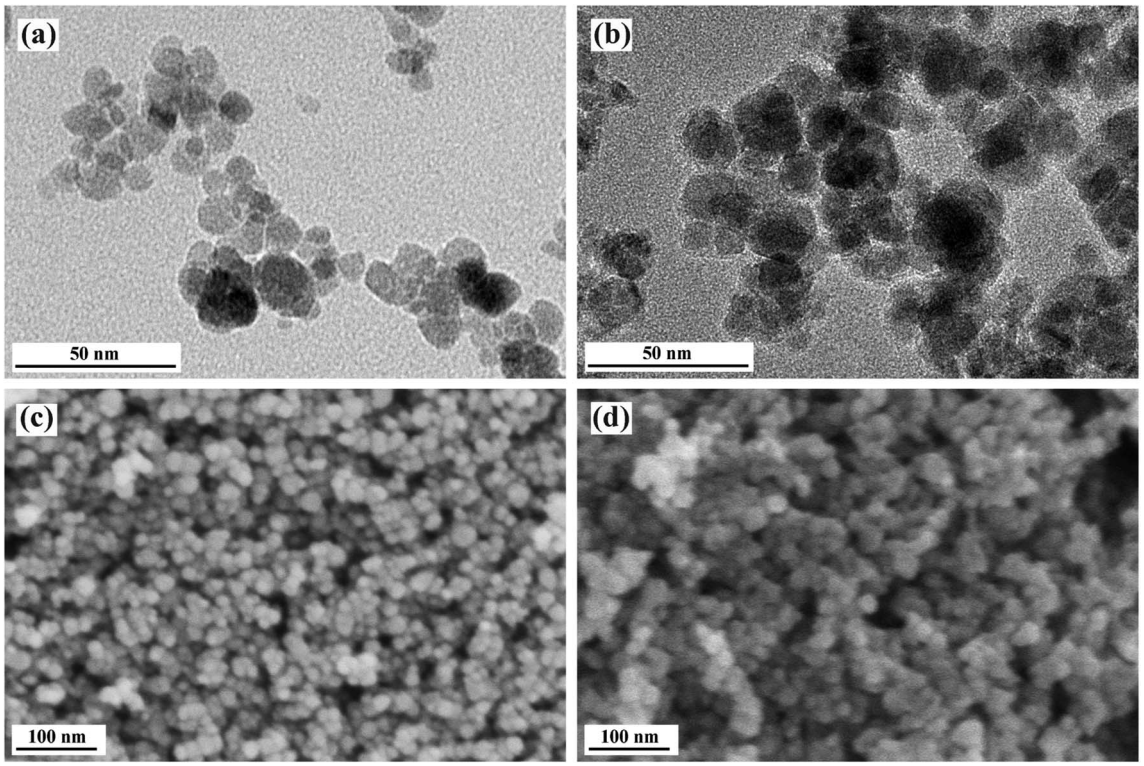

Fig. 3 TEM images of: (a) Fe_3O_4 NPs and (b) PK-Fe_3O_4 NPs. SEM images of: (c) Fe_3O_4 NPs and (d) PK-Fe_3O_4 NPs.

2.6. Interfacial tension test and contact angle measurement

To investigate the influences of PK-Fe_3O_4 NFs on the oil–water interfacial properties, the IFT of water–oil and NFs–oil systems were tested by Optical Contact Angle & Interface Tension Meter (SL200KS) by pendant drop method at ambient temperature.

2.6.1. IFT tests. In this study, the sessile drop method was used to test the IFT between bitumen and NFs. To improve the mobility of bitumen at ambient temperature, the bitumen was diluted to 10 wt% by toluene during the test. The diluted bitumen was injected into the NFs using a U-shape bent needle fixed on a micro-syringe. The tension meter was applied to capture the profile of diluted-bitumen drops in alkali water or PK-Fe_3O_4 NFs. The images were captured and analyzed by fitting drop shape profile, obtaining the IFT.[23,44]

2.6.2. Contact angle measurements. Wettability alteration of minerals by PK-Fe_3O_4 NFs was monitored by measuring droplet contact angles of water contact on NPs-coated glass in air and water contact on bare glass in air at ambient temperature. To control the surface hydrophobicity of the glass surface, the first step was to make a clean and untreated glass surface. To prevent contamination, a glass plate of 2.5 cm × 2.5 cm × 0.2 cm was treated by 2 wt% SDS solution under ultrasonication for 10 min, followed by washing with deionized water for twice. The prepared clean glass plate was dipped completely in PK-Fe_3O_4 NPs for 72 h to ensure equilibrium conditions. The surface was then dried at room temperature in a dust-free atmosphere. The manual experimental setup consists of the glass plate, a micro-syringe and the tension meter. Initially, the glass plate was placed on the sample stage horizontally. Thereafter, the DI water was injected using the micro-syringe. The micro-syringe was gently adjusted to make the water drop attach to the glass plate beneath. The shape of the water drop on the plate was captured by the camera of the tension meter, which was then analyzed to obtain the contact angle.[44] Every measurement was repeated at least three times for reproducibility.

3. Results and discussion

3.1. Characterizations of PK-Fe_3O_4 nanoparticles

The morphology and distribution of the nano products are examined by TEM and SEM. Fig. 3 shows TEM images of Fe_3O_4 NPs and PK-Fe_3O_4 NPs, which appear as spherical contour and even some aggregations. The average diameters of Fe_3O_4 NPs and PK-Fe_3O_4 NPs are about 10.41 and 15.89 nm, respectively. Due to the entanglement of long chains of PEG, there appears an adhesion phenomenon between PK-Fe_3O_4 NPs, shown in Fig. 3c and d.

FT-IR spectra of PK molecules, KH560 and PEG600 are shown in Fig. 4a. FT-IR spectra of PEG600 consists of stretching vibration of –OH groups at ~3500 cm^{-1} and symmetrical stretching vibration of $-CH_2$ groups at ~2900 cm^{-1} and 1250–1500 cm^{-1}. They are also observed in PK spectra. The strong absorption peak at ~1100 cm^{-1} assigned to C–O–C groups is also detected in PK spectra. FT-IR spectra of KH560 contains stretching vibration absorption peaks for C–H at 2800–3000 and

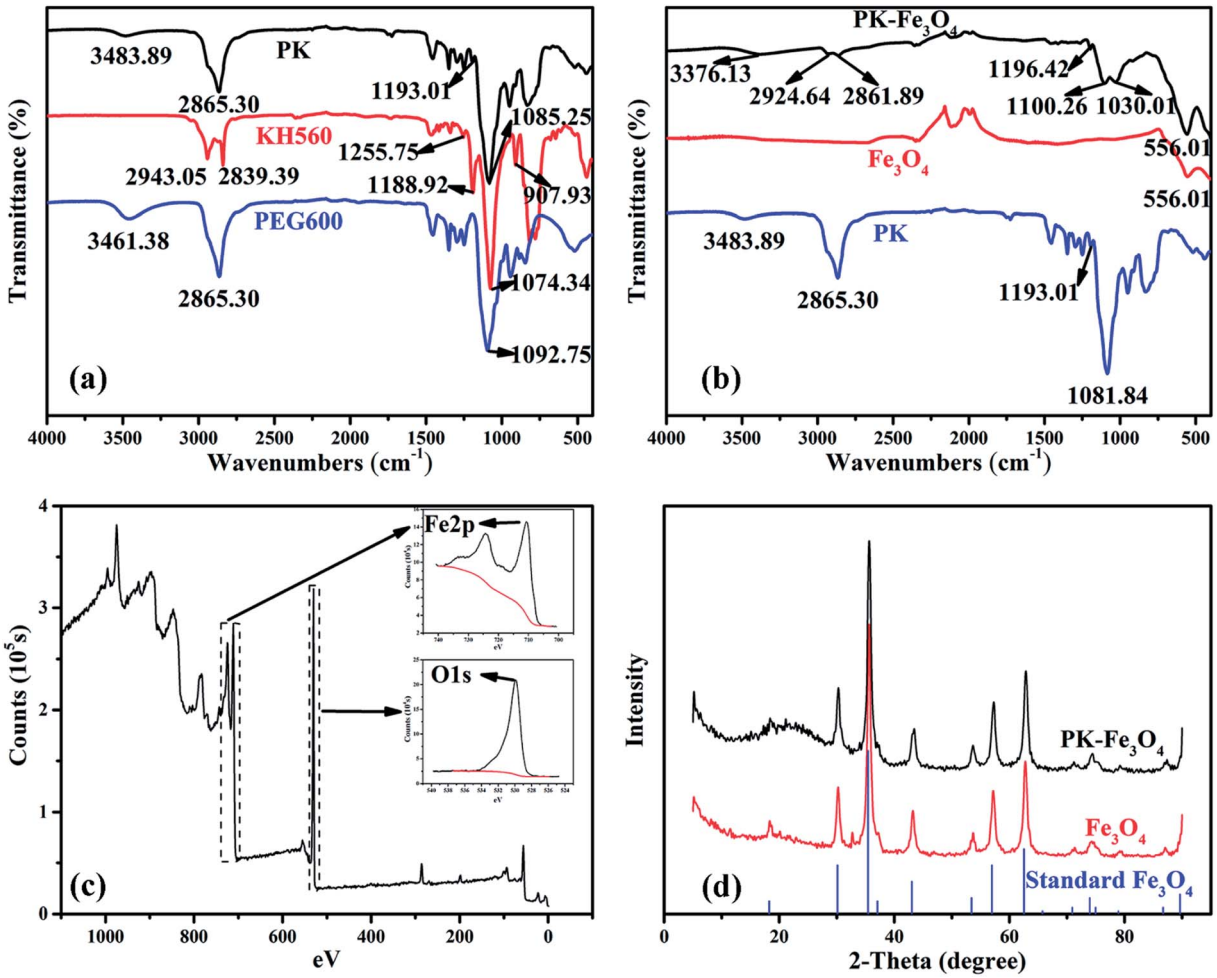

Fig. 4 (a) FT-IR spectra of PK, KH560 and PEG600; (b) FT-IR spectra of PK-Fe_3O_4, Fe_3O_4 and PK; (c) XPS broad scan spectra of Fe_3O_4 NPs, and the insets are narrow scan for Fe 2p and O 1s; (d) XRD patterns of standard diffraction peaks, Fe_3O_4 NPs and PK-Fe_3O_4 NPs.

1250–1500 cm^{-1}. The peaks at ~1200 cm^{-1} and ~1100 cm^{-1}, assigned to Si–O–C and C–O–C groups, respectively, are also observed in PK FT-IR spectra. While absorption peaks referred to epoxy ring at 1250 and 890 cm^{-1} do not appear in PK spectra.[45] The appearance of Si–O–C groups peak and disappearance of the epoxy ring peak in PK FT-IR spectra reveal that the addition reaction happens (shown by eqn (2)).

FT-IR spectra of PK-grafted Fe_3O_4 NPs, unmodified Fe_3O_4 nanoparticle and PK molecules are depicted in Fig. 4b. Absorption peaks at ~3400 cm^{-1}, ~2900 cm^{-1}, ~1200 cm^{-1}, ~1100 cm^{-1} and ~550 cm^{-1} are assigned to the stretching vibrations of –OH groups, symmetrical stretching vibration of $–CH_2$ groups, Si–O–C groups, C–O–C groups and stretching vibration of Fe–O bonds, respectively. It is worth noting that the absorption peak of asymmetrical stretching vibration of $–CH_2$ groups at ~2900 cm^{-1}, which is partially covered by the strong adsorption peak of symmetrical stretching vibration, relatively strengthens due to the grafting reaction. This phenomenon also acts on the primary alcohol absorption peak belonging to PEG600 molecules and open-looped KH560 at ~1050 cm^{-1}, which is covered by the strong adsorption peak of C–O–C groups in the spectra of PEG600 and PK.[46] These results indicate that PK has been grafted on the surface of Fe_3O_4 NPs successfully.

Fig. 4c presents the broad and narrow scan XPS spectra of Fe_3O_4 NPs. The peaks at 711.0 eV, 724.0 eV and 529.9 eV are the characteristic doublets of Fe $2p_{3/2}$, Fe $2p_{1/2}$ and O 1s from iron oxide, respectively, which is consistent with the reported values of Fe_3O_4.[40]

Fig. 4d shows the XRD patterns of standard diffraction peaks of PK-Fe_3O_4 NPs, Fe_3O_4 NPs and face-centered cubic Fe_3O_4 phase (JCPDS card 19-629).[47] The diffraction peaks in Fe_3O_4 NPs are basically the same as the standard ones. Generally, the addition of grafted groups will bring out new diffraction peaks. However, results of XRD tests show that the peak positions of diffractive peaks before and after grafting reaction are basically the same. The result suggests that there is no crystal transformation of Fe_3O_4 NPs during the grafting reaction. It also indicates that the grafted groups may be amorphous.

Magnetic characterizations of Fe_3O_4 NPs and PK-Fe_3O_4 NPs have been tested in the physical property measurements system of VSM at ambient temperature. It was conducted with a magnetic field in the range of −10 000 to 10 000 Oe, where the

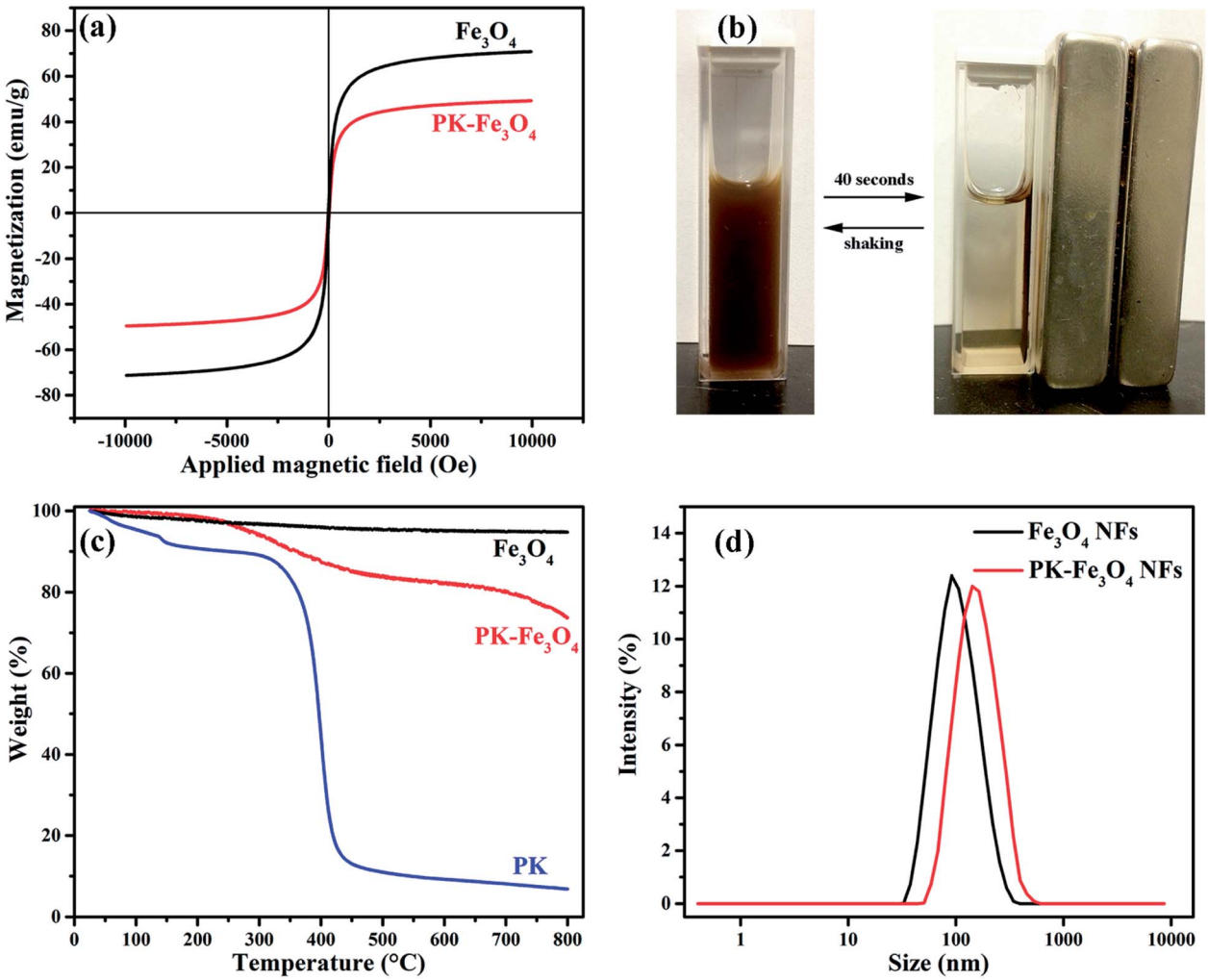

Fig. 5 (a) Magnetic hysteresis loops of Fe_3O_4 NPs and PK-Fe_3O_4 NPs at ambient temperature; (b) experimental phenomena of magnetic separation and redispersion of PK-Fe_3O_4 NPs; (c) TG thermograms of Fe_3O_4, PK-Fe_3O_4 and PK; (d) size distribution of Fe_3O_4 NFs and PK-Fe_3O_4 NFs.

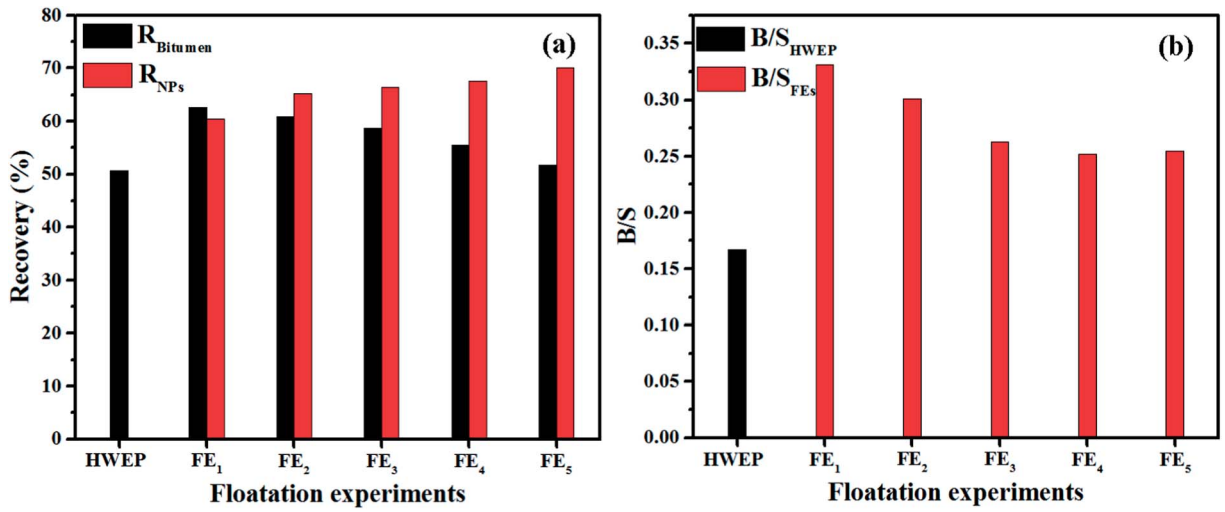

Fig. 6 (a) Recovery of bitumen and NPs in floatation experiments and (b) the corresponding B/S of froth from different extractions.

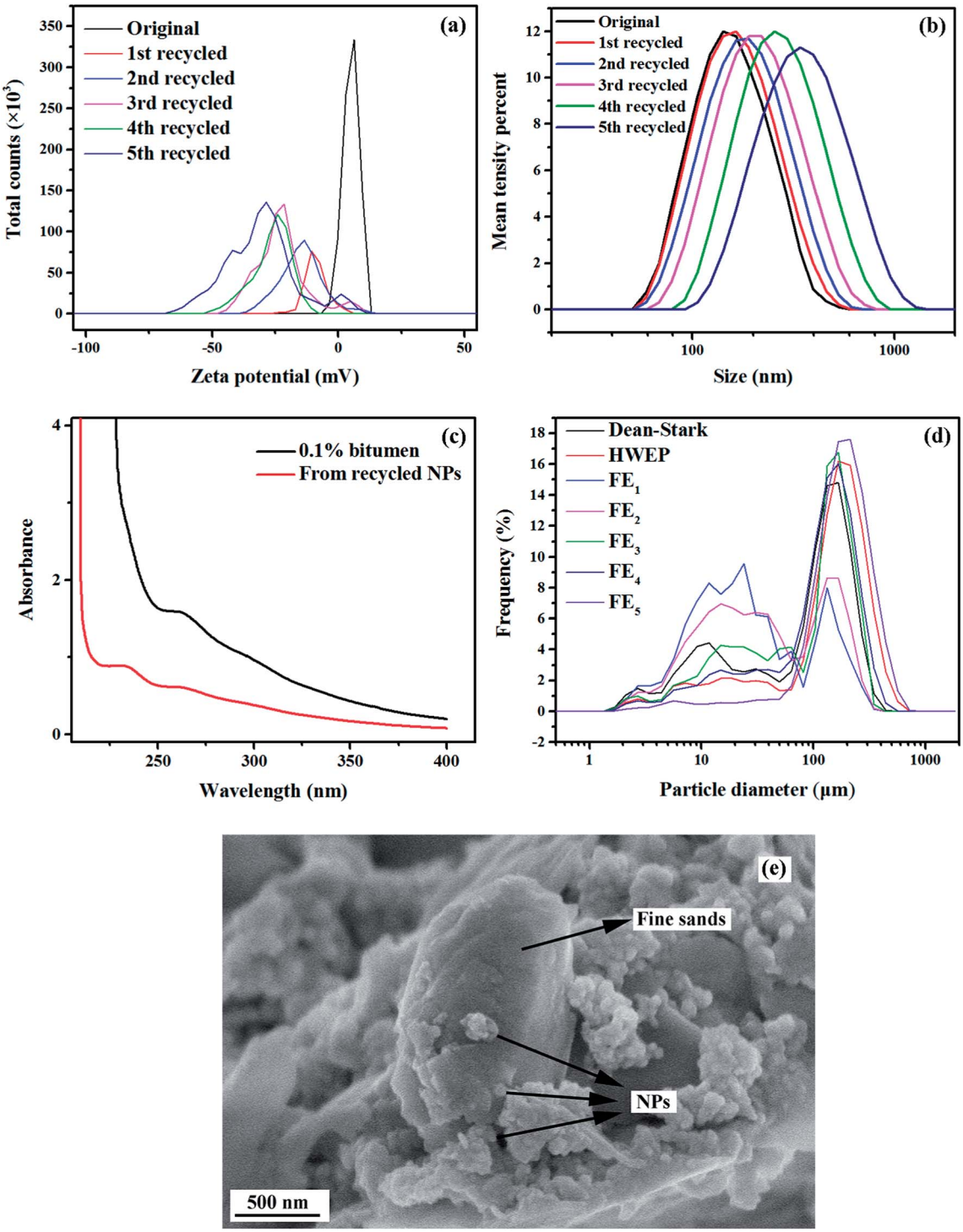

Fig. 7 (a) Zeta potentials of NFs; (b) size distributions of NFs; (c) UV-vis absorption spectrum of bitumen and components from recycled NPs; (d) LPSA tests of sands from bitumen froth; (e) SEM image of recovered PK-Fe_3O_4 NPs.

influence of saturation magnetization (M_s), and coercive field (H_c) are evaluated. The Fe_3O_4 powders usually show a super-paramagnetic behavior, because each of the particles can be treated as a thermally agitated permanent magnet. This type of materials often shows hysteresis loops (M–H curves). Fig. 5a shows that the M_s values of Fe_3O_4 NPs and PK-Fe_3O_4 NPs are 70.85 and 49.36 emu g^{-1}, respectively. The appearance of magnified hysteresis loops further confirms the super-paramagnetism of these particles. While, the reduction in saturation magnetization of PK-Fe_3O_4 NPs suggest that the grafting of PK on the particle surface would weaken the magnetism of the nanoparticles.

The magnetic separation experiment (shown in Fig. 5b) exhibits that PK-Fe_3O_4 NPs could be dispersed in water by

Table 1 Substance concentrations (wt%, in the form of oxide) from the froth of HWEP and FEs

	Al_2O_3	Fe_3O_4	K_2O	P_2O_5	SiO_2	SO_3	TiO_2	Others
HWEP	11.30	**1.55**	1.89	1.29	80.29	1.65	1.10	2.03
FEs	11.12	**3.31**	2.51	1.30	76.73	1.48	1.64	3.55

shaking or ultrasonication to form a stable suspension without settlement or aggregation in 72 h. When the magnetic field was applied, the particles could be quickly separated from the solution. If the magnetic field was removed, these collected particles could be dispersed in the solution again. These results show that the PK-Fe_3O_4 NPs possess excellent magnetic responsivity and redispersibility, which is important in terms of their practical application.

In the TGA analysis, shown in Fig. 5c, the weight of synthesized Fe_3O_4 NPs is found to be almost unchanged during heating to 800 °C. However, after grafting reaction, PK-Fe_3O_4 NPs appear a mass loss at about 200 °C, with weight loss of about 17%. The temperature interval of the weight loss is similar to that of PK molecules, whose weight loss is more than 75% from 300 °C to 500 °C. The weight loss is also in accordance with the saturation magnetization difference between bare Fe_3O_4 and PK-Fe_3O_4 (from 70.85 to 49.36 emu g^{-1}). These results further verify that the PK has been grafted on Fe_3O_4 NPs surface successfully.

Fig. 5d demonstrates the hydraulic diameter and dispersibility of Fe_3O_4 NPs and PK-Fe_3O_4 NPs. Results show that the average hydraulic diameter of Fe_3O_4 NPs is at 105.7 nm with a polydispersibility index (PDI) of 0.107, while the diameter and PDI become 142.0 nm and 0.150, respectively, for PK-Fe_3O_4 NPs.

Table 2 Distribution of PK-Fe_3O_4 NPs after FEs

Sources of NPs	Solution	Residual solids[a]	Bitumen froth
Concentration (wt%)	70.04	20.21	9.75

[a] These NPs are attached on the residual solid surfaces.

It suggests that the grafting of PK results in the increase in the hydraulic diameter.[32]

3.2. Application in oil sands separation

Results of heavy oil recovery from oil sands by PK-Fe_3O_4 NFs are given in Fig. 6. At given conditions, the PK-Fe_3O_4 NFs could achieve 62.61% of the oil recovery by single extraction step, over 12% more than that of traditional hot water extraction process (HWEP) without NPs addition, shown in Fig. 6a. In addition, the bitumen to solid ratio (B/S) of oil product is also found to be improved by the PK-Fe_3O_4 NFs (0.33) compared with that of the HWEP (0.18), given in Fig. 6b. These results suggest that the addition of PK-Fe_3O_4 NPs would increase the quality of bitumen froth. One of the major advantages of the magnetic NPs is their magnetic response which allows them to be recyclable. Herein, after the extraction, the PK-Fe_3O_4 NPs are recycled for further use. It is found that up to 70% of the PK-Fe_3O_4 NPs could be directly recycled from the solution for further extraction. The rest of the NPs are found to be left in the oil phase and attached in the residual solids. Further recycling tests show that the oil recovery decreases from 62.62% to 51.70% when the cycling time increases from 2 to 5, shown in Fig. 6a. The B/S also reduces from 0.33 to 0.25 from the 1st floatation experiment (FE_1) to the 5th floatation experiment (FE_5), shown in Fig. 6b. However, the recycled NPs increases from 60.40% to 70.04% during the recycling accordingly.

To understand why increasing the recycling times reduces the extraction efficiency of PK-Fe_3O_4 NFs, further tests were conducted. Fig. 7a presents the zeta potential of the original PK-Fe_3O_4 NPs and recycled NPs at different stages. Obviously, the zeta potentials of NPs change from positive (original NPs before extraction) to negative (as low as −50 mV) when increasing the recycling times. The more the cycling times, the more negatively charged the NPs. Fig. 7b shows that the hydrodynamic diameter of NPs grows a little bit after recycling. This growth of the nanoparticle size is ascribed to the adsorption of some oil components on the nanoparticle surfaces. The adsorbed oil components on the NPs surfaces were found to be dissolved in cyclohexane. As shown in Fig. 7c, the UV-vis test shows that the obtained cyclohexane solution exhibits similar absorption peaks with bitumen dissolved in cyclohexane (0.1%), suggesting

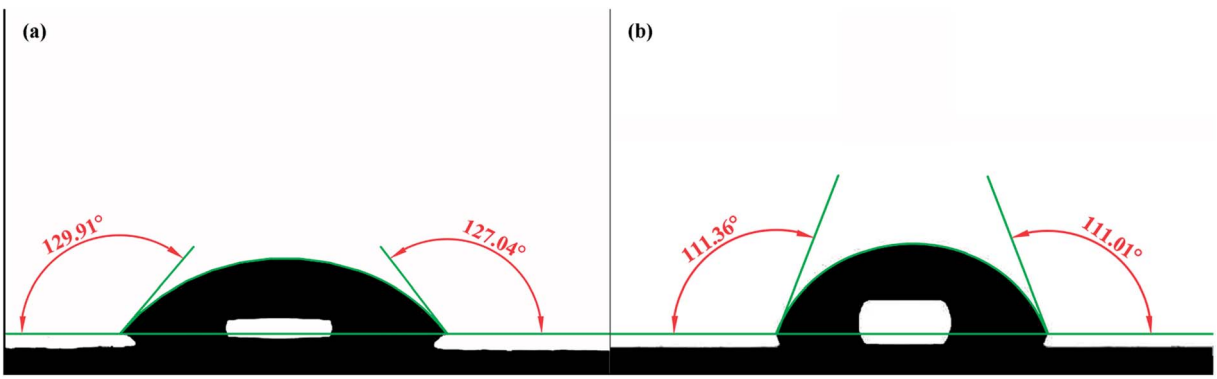

Fig. 8 Contact angles of water on (a) NPs-coated glass and (b) bare glass in air.

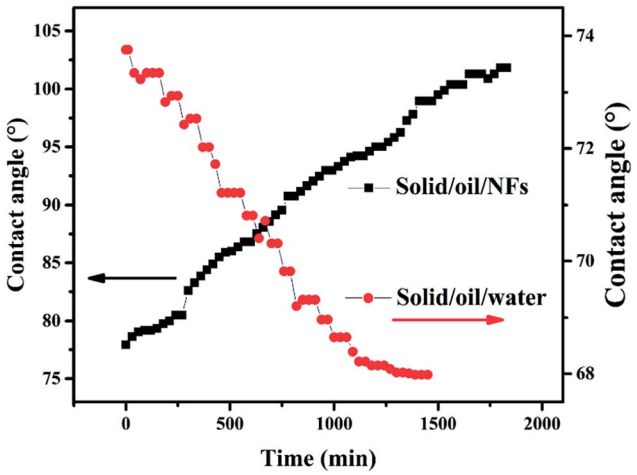

Fig. 9 Dynamic contact angles of solid/oil/NFs and solid/oil/water in 24 h.

the appearance of oil component on the nanoparticle surfaces. Future study will be conducted to detect the exact chemical composition of the adsorbed materials.

In Fig. 7e, it is found that some of the NPs are adsorbed on the fine solids (diameter < 44 μm). The adsorption of NPs on mineral surfaces may be ascribed to the strong interaction between surface hydroxyls of minerals and C–O–H bonds of NPs.[48] This adsorption brings the minerals to the recycled PK-Fe_3O_4 NPs, leading to the reduction of the efficiency of the PK-Fe_3O_4 NPs. This entrainment of fine solids by the PK-Fe_3O_4 NPs is further confirmed by the reduced fines in the bitumen froth during the recycling of NPs through Laser Particle Size Analyzer (LPSA) test, shown in Fig. 7d. Similarly, the adsorption of PK-Fe_3O_4 NPs on the mineral surfaces would also bring some NPs into the bitumen froth. As shown in Table 1, the content of Fe_3O_4 in the froth entrained minerals increased from 1.55 wt% to 3.31 wt%. This is also the reason there is some loss of Fe_3O_4 during the extraction. Moreover, the distribution of NPs from the floatation experiment is shown in Table 2.

3.3. Roles of PK-Fe_3O_4 NPs in EOR

The newly synthesized PK-Fe_3O_4 NPs are proven to be beneficial for the heavy oil recovery from oil sands. Basically, the NPs play two important roles in modifying the oil surface and the mineral surface. For the mineral surfaces, during the extraction, the PK-Fe_3O_4 NPs are found to be adsorbed on the mineral surfaces, shown in Fig. 7e. To further find out how the nanoparticle adsorption influences the mineral, contact angle measurements are applied for water on NPs-coated glass in air and on bare glass as mentioned in Section 2.6. Fig. 8a and b show that the water contact angle on NPs-coated glass (128.48°) in air is larger than that on bare glass surface (111.18°). It indicates that the coating of PK-Fe_3O_4 NPs increases the hydrophilicity of the glass surface. The increase of the hydrophilicity of minerals surface will facilitate the liberation of oil from the mineral surface.[10,13,14]

For the purpose of making a close observation on the adsorption effect of NPs on the surface of solids, the dynamic contact angles of solid/oil/NFs and solid/oil/water have been measured. The glass plate were selected as the model of mineral solid surface. The plate was firstly immersed in petroleum ether for 12 h to form an oil-wet surface. Toluene-diluted bitumen (1.0 wt%) was chosen as the oil phase. Results in Fig. 9 show that the contact angle of solid/oil in NFs increases from 77.92° to 101.87°, which is in accordance with the reported phenomenon.[27] This increase in contact angle suggests the adsorption of nanoparticles on the solid surface. Because of the adsorption of NPs on the surface of solids, the force of the wedge structure pressure "squeezes" the contact line of NFs/oil. In addition, assisted by the mechanical disturbance from the agitator, the

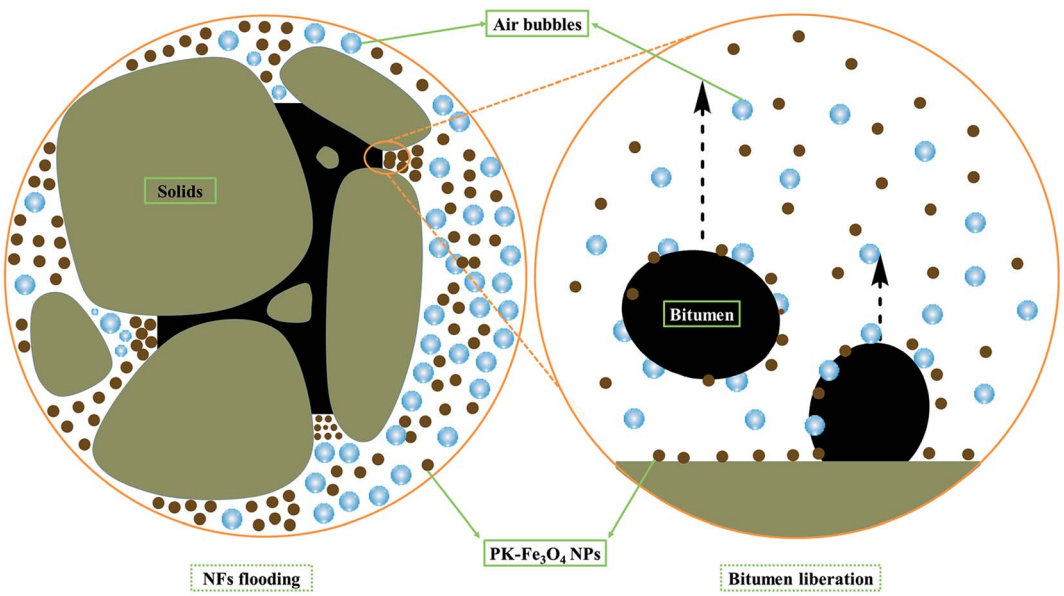

Fig. 10 Microscopic sketch of the liberating process.

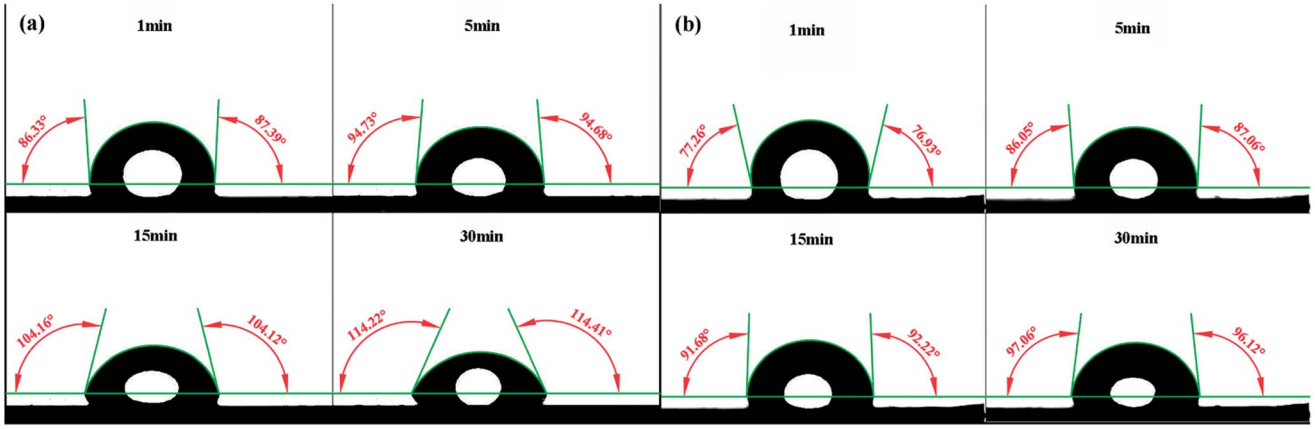

Fig. 11 Changes of (a) NFs contact angle and (b) water contact angle on oil over 30 min.

bitumen is easier to be removed from the surface of sands.[49] The liberated bitumen is then entrained by air bubbles to form the bitumen froth. Fig. 9 also presents that the contact angle of solid/oil in water decreases from 73.75° to 67.98°. The reverse in tendency with contact angle of solid/oil/NFs is ascribed to that pure water can only provide interfacial tension at the vertex of the contact area. Under the action of buoyancy force, the oil droplet slowly spreads to the glass plate. The microscopic sketch of the liberating process is shown in Fig. 10.

For the oil surfaces, the addition of PK-Fe_3O_4 NPs is found to be able to significantly reduce the oil–water interfacial tension. Fig. 11a and b present the changes of NFs and water contact angles on bitumen-coated glass surface. It is obvious that the water contact angle on oil in air increases from 77.10° to 96.59°. While it changes from 86.86° to 114.32° for PK-Fe_3O_4 NFs on oil in air. This result suggests that the addition of PK-Fe_3O_4 NPs allows the bitumen surface more hydrophilic. On the other hand, the addition of PK-Fe_3O_4 NPs in the solution also reduces the heavy oil–water interfacial tension from 14.40 mN m^{-1} to 8.59 mN m^{-1}. This finding indicates that the PK-Fe_3O_4 NPs act as a role of 'surfactant' in NFs. Owing to the cyclic hydrophilic groups C–O–C and hydrophobic groups CH_2–CH_2 in PEG molecules, they possess good intermiscibility in water with alkane groups in heavy oil. Declining IFT results in a reduction in capillary pressure that reveals to better efficiency and further aids the oil liberation process.[19] The above roles of PK-Fe_3O_4 NPs contribute to the enhanced oil recovery from oil sands.

It should be mentioned that although the addition of PK-Fe_3O_4 NPs could enhance the oil sands separation, its efficiency would be reduced when directly recycling the PK-Fe_3O_4 NPs due to the adsorption of oil components. Therefore, the PK-Fe_3O_4 NPs should be treated by solvent washing to remove the oil components before its next application in extraction.

4. Conclusions

Here, PEG coated hydrophilic nanoparticle (PK-Fe_3O_4 NPs) has been synthesized by co-precipitation and surface group grafting reaction. This kind of nanoparticle is averaged at around 16 nm in size. It could be well dispersed in water, forming stable PK-Fe_3O_4 NFs. The superparamagnetic property of PK-Fe_3O_4 NPs enables them to be separated by external magnetic fields, facilitating their recycling and reusing. The results of floatation experiments by PK-Fe_3O_4 NFs reveal that an extra oil recovery of 12% can be achieved with the improvement in the quality of bitumen froth (B/S). It is found that up to 70% of the PK-Fe_3O_4 NPs could be directly recycled from the solution for further use. The rest NPs are leaving in the oil phase and attached on the residual solid surface. However, because there are some oil components being adsorbed on the NPs surfaces, it is observed that the efficiency of PK-Fe_3O_4 NPs will be reduced to some extent when recycling them without treatment for further extraction. This enhancement of PK-Fe_3O_4 NPs in oil recovery from unconventional oil ores would be contributed by two roles: the adsorption of PK-Fe_3O_4 NPs on mineral surface, resulting in the increased wettability of the mineral surfaces; and the alternation of the oil–water interface, allowing the reduction in oil–water IFT. However, it should be mentioned that the adsorption of NPs on surfaces of minerals would also lead to the loss of PK-Fe_3O_4 NPs in the oil phase, and the deterioration of the NPs due to the entrainment of minerals in the recycled NPs. In addition, the adsorption of oil components on the NPs surface implies that the PK-Fe_3O_4 NPs should not be directly recycled but solvent washed before next extraction.

Conflicts of interest

There are no conflicts to declare.

Acknowledgements

This work was financially supported by National Natural Science Foundation of China (NSFC, No. 21506155, No. 41471258).

References

1 K. Guo, H. Li and Z. Yu, *Fuel*, 2016, **185**, 886–902.

2 H. Ma, G. Yu, Y. She and Y. Gu, *J. Pet. Sci. Eng.*, 2017, **149**, 465–475.
3 H. Pei, G. Zhang, J. Ge, P. Jiang, J. Zhang and Y. Zhong, *Colloids Surf., A*, 2017, **529**, 409–416.
4 M. Safdel, M. A. Anbaz, A. Daryasafar and M. Jamialahmadi, *Renewable Sustainable Energy Rev.*, 2017, **74**, 159–172.
5 M. Nabipour, S. Ayatollahi and P. Keshavarz, *J. Mol. Liq.*, 2017, **230**, 579–588.
6 M. Mohebbifar, M. H. Ghazanfari and M. Vossoughi, *J. Energy Resour. Technol.*, 2015, **137**, 014501.
7 N. A. Ogolo, O. A. Olafuyi and M. O. Onyekonwu, *Soc. Pet. Eng. J.*, 2012, 875–885.
8 F. Bordeaux Rego, V. E. Botechia and D. J. Schiozer, *J. Pet. Sci. Eng.*, 2017, **153**, 187–196.
9 S. M. Seyyedsar and M. Sohrabi, *Fuel Process. Technol.*, 2017, **164**, 1–12.
10 X. Sun, Y. Zhang, G. Chen and Z. Gai, *Energies*, 2017, **10**, 345.
11 A. Zhong, *Challenges for High-Pressure High-Temperature Applications of Rubber Materials in the Oil and Gas Industry*, Springer International Publishing, Cham, 2016, pp. 65–79.
12 J. Yang, S. Ji, R. Li, W. Qin and Y. Lu, *Energy Explor. Exploit.*, 2015, **33**, 639–657.
13 M. S. Kamal, A. A. Adewunmi, A. S. Sultan, M. F. Al-Hamad and U. Mehmood, *J. Nanomater.*, 2017, **2017**, 15.
14 J. Giraldo, P. Benjumea, S. Lopera, F. B. Cortés and M. A. Ruiz, *Energy Fuels*, 2013, **27**, 3659–3665.
15 A. Karimi, Z. Fakhroueian, A. Bahramian, N. Pour Khiabani, J. B. Darabad, R. Azin and S. Arya, *Energy Fuels*, 2012, **26**, 1028–1036.
16 R. Nazari Moghaddam, A. Bahramian, Z. Fakhroueian, A. Karimi and S. Arya, *Energy Fuels*, 2015, **29**, 2111–2119.
17 A. Maghzi, S. Mohammadi, M. H. Ghazanfari, R. Kharrat and M. Masihi, *Exp. Therm. Fluid Sci.*, 2012, **40**, 168–176.
18 S. Kiani, M. Mansouri Zadeh, S. Khodabakhshi, A. Rashidi and J. Moghadasi, *Energy Fuels*, 2016, **30**, 3791–3797.
19 A. Ahmed, I. Mohd Saaid, A. H. Tunio, R. Pilus, M. Mumtaz and I. Ahmad, *J. Appl. Environ. Biol. Sci.*, 2017, **7**, 56–62.
20 R. Songolzadeh and J. Moghadasi, *Colloid Polym. Sci.*, 2016, **295**, 145–155.
21 B. Ju, T. Fan and M. Ma, *China Particuol.*, 2006, **4**, 41–46.
22 T. Sharma, S. Iglauer and J. S. Sangwai, *Ind. Eng. Chem. Res.*, 2016, **55**, 12387–12397.
23 L. He, F. Lin, X. Li, Z. Xu and H. Sui, *Energy Fuels*, 2014, **28**, 7403–7410.
24 B. A. Suleimanov, F. S. Ismailov and E. F. Veliyev, *J. Pet. Sci. Eng.*, 2011, **78**, 431–437.
25 Y. Wang, W. Jia, M. Ding, H. Yang, B. Hu and S. Ren, *Energy Fuels*, 2012, **26**, 1019–1027.
26 C. Dai, X. Wang, Y. Li, W. Lv, C. Zou, M. Gao and M. Zhao, *Energy Fuels*, 2017, **31**, 2663–2668.
27 D. T. Wasan and A. D. Nikolov, *Nature*, 2003, **423**, 156–159.
28 H. Zhang, A. Nikolov and D. Wasan, *Energy Fuels*, 2014, **28**, 3002–3009.
29 L. He, F. Lin, X. Li, H. Sui and Z. Xu, *Chem. Soc. Rev.*, 2015, **44**, 5446–5494.
30 J. A. Darr, J. Zhang, N. M. Makwana and X. Weng, *Chem. Rev.*, 2017, **117**, 11125–11238.
31 S. Xuan, Y. X. Wang, J. C. Yu and K. C. Leung, *Langmuir*, 2009, **25**, 11835–11843.
32 J. Xie, C. Xu, N. Kohler, Y. Hou and S. Sun, *Adv. Mater.*, 2007, **19**, 3163–3166.
33 A. Ito, M. Shinkai, H. Honda and T. Kobayashi, *J. Biosci. Bioeng.*, 2005, **100**, 1–11.
34 A. Behzadi and A. Mohammadi, *J. Nanopart. Res.*, 2016, **18**, 266.
35 W. Yu and H. Xie, *J. Nanomater.*, 2012, **2012**, 1–17.
36 H. ShamsiJazeyi, C. A. Miller, M. S. Wong, J. M. Tour and R. Verduzco, *J. Appl. Polym. Sci.*, 2014, **131**, 4401–4404.
37 S. K. Choi, H. A. Son, H. T. Kim and J. W. Kim, *Energy Fuels*, 2017, **31**, 7777–7782.
38 X. Liang, X. Wang, J. Zhuang, Y. Chen, D. Wang and Y. Li, *Adv. Funct. Mater.*, 2006, **16**, 1805–1813.
39 Z. Lin, Z. Zhang, Y. Li and Y. Deng, *Chem. Eng. J.*, 2016, **288**, 305–311.
40 G. H. Du, Z. L. Liu, X. Xia, Q. Chu and S. M. Zhang, *J. Sol-Gel Sci. Technol.*, 2006, **39**, 285–291.
41 C. Anushree and J. Philip, *J. Mol. Liq.*, 2016, **222**, 350–358.
42 L. Qiu, MS thesis, University of Alberta, 2010.
43 F. Lin, L. He, J. Hou, J. Masliyah and Z. Xu, *Energy Fuels*, 2016, **30**, 121–129.
44 S. Velusamy, S. Sakthivel and J. S. Sangwai, *Ind. Eng. Chem. Res.*, 2017, **56**, 13521–13534.
45 J. Coates, Interpretation of infrared spectra, a practical approach, *Encyclopedia of analytical chemistry*, Wiley, Chichester, 2000.
46 S. Xuan, F. Wang, J. M. Lai, K. W. Sham, Y. X. Wang, S. F. Lee, J. C. Yu, C. H. Cheng and K. C. Leung, *ACS Appl. Mater. Interfaces*, 2011, **3**, 237–244.
47 M. Shao, F. Ning, J. Zhao, M. Wei, D. G. Evans and X. Duan, *J. Am. Chem. Soc.*, 2012, **134**, 1071–1077.
48 X. Li, Y. Bai, H. Sui and L. He, *Energy Fuels*, 2017, **31**, 1174–1181.
49 A. J. Lynch, J. S. Watt and G. Harbort, *History of Flotation Technology*, Littleton, 2007.